Journal of Materials Chemistry A

ROYAL SOCIETY OF CHEMISTRY

PAPER

Cite this: *J. Mater. Chem. A*, 2021, **9**, 26202

Efficient separation of xylene isomers by using a robust calcium-based metal–organic framework through a synergetic thermodynamically and kinetically controlled mechanism†

Yuhan Lin,‡[a] Jian Zhang,‡[a] Haardik Pandey,‡[b] Xinglong Dong,[c] Qihan Gong,[d] Hao Wang,*[a] Liang Yu,[a] Kang Zhou,[a] Wei Yu,[a] Xiaoxi Huang,[a] Timo Thonhauser,[b] Yu Han*[c] and Jing Li*[ea]

Received 19th September 2021
Accepted 4th November 2021

DOI: 10.1039/d1ta08055e

rsc.li/materials-a

Adsorptive separation of physically and chemically similar molecules and understanding the underlying host–guest interactions at the molecular level are of significant scientific and practical importance. Here we report the development of a novel calcium-based metal–organic framework, formulated as $Ca_3(Htcpp)_2$ (H_4tcpp = 2,3,5,6-tetrakis(4-carboxyphenyl)-pyrazine) featuring microporosity and high stability. This compound shows distinct adsorption behavior toward xylene isomers and is capable of separating them efficiently at an industrially relevant temperature. The selective adsorption is attributed to a synergetic thermodynamic and kinetic effect. The host–guest interactions were probed directly by single-crystal X-ray diffraction analysis and the adsorption affinity was evaluated through computational molecular simulations.

Introduction

Adsorptive separation of highly similar hydrocarbon molecules is considered as a challenging yet promising alternative technology to traditional distillations, due to the lower energy cost and reduced carbon dioxide emission associated with this technology. It is, therefore, of great industrial importance.[1] Xylene isomers, particularly *o*-xylene and *m*-xylene, are of the highest level of separation complexity as a result of their extremely similar physical and chemical properties. The boiling point, polarizability and dipole moment of the three isomers, *p*-xylene, *m*-xylene, and *o*-xylene (denoted as *p*X, *m*X, and *o*X, respectively), follow the sequence of *o*X > *m*X ≈ *p*X, but the differences are minimal. Shape-selective adsorption has been realized by certain adsorbents, including zeolites and metal–organic frameworks (MOFs), for the separation of *p*X from *m*X and *o*X, by taking advantage of the relatively slim geometry of *p*X and its smaller kinetic diameter (5.8 Å for *p*X *vs.* 6.8 Å for *m*X and *o*X).[2]

Compared to traditional inorganic and organic adsorbents, MOFs are intrinsically advantageous for the separation of physically similar molecules, including xylene isomers, because of their diverse structures and tunable pore size/shape.[3] Zhang *et al.* reported a MOF, $Cu_2(pypz)_2$ (Hpypz = 4-(1*H*-pyrazol-4-yl) pyridine), with tunable structural flexibility.[4] It selectively adsorbs *p*X over *m*X and *o*X with a selectivity as high as 51. Zhu *et al.* developed a microporous MOF, In(OH)(OBA) (H_2OBA = 4,4′-oxybis(benzoic acid)), which adsorbs *p*X only but fully excludes *m*X and *o*X, acting as a molecular sieve.[5] The separation of *m*X and *o*X is more challenging because of their similar shape and size. Zaworotko *et al.* reported a flexible MOF, sql-1-Co-NCS, that can discriminate between *m*X and *o*X owing to their different gate-opening pressures, with *o*X as the preferentially adsorbed isomer.[6] Selective adsorption of *o*X over *m*X has also been observed for Co_2(dobdc), Co_2(*m*-dobdc),[7] MIL-53(Cr),[8] CD-MOF-1,[9] and the recently reported ZU-61.[10] Preferential adsorption of *o*X on these materials could be attributed to its higher polarizability and dipole moment, leading to higher adsorption affinity to MOFs. Comparatively, MOFs showing selective adsorption of *m*X over *o*X are relatively rare. Yang and Schröder *et al.* recently reported the separation of xylene isomers using the MFM-300(M) (M = In, V, Fe, Al) family,

[a]*Hoffmann Institute of Advanced Materials, Shenzhen Polytechnic, 7098 Liuxian Boulevard, Shenzhen, Guangdong 518055, P. R. China. E-mail: wanghao@szpt.edu.cn*

[b]*Department of Physics, Center for Functional Materials, Wake Forest University, Winston-Salem, NC 27109, USA*

[c]*Advanced Membranes and Porous Materials Center, Physical Sciences and Engineering Division, King Abdullah University of Science and Technology, Thuwal 23955-6900, Saudi Arabia. E-mail: yu.han@kaust.edu.sa*

[d]*Fundamental Science & Advanced Technology Lab, PetroChina Petrochemical Research Institute, Beijing 102200, P. R. China*

[e]*Department of Chemistry and Chemical Biology, Rutgers University, 123 Bevier Road, Piscataway, New Jersey 08854, USA. E-mail: jingli@rutgers.edu*

† Electronic supplementary information (ESI) available. CCDC 2093140–2093143. For ESI and crystallographic data in CIF or other electronic format see DOI: 10.1039/d1ta08055e

‡ These authors contributed equally to this work.

exhibiting adsorption preference following the sequence of *m*X > *o*X > *p*X as a result of cooperative supramolecular binding interactions.[11] In this work we report a new microporous calcium-based MOF, $Ca_3(Htcpp)_2$ (denoted as HIAM-201, where HIAM refers to Hoffmann Institute of Advanced Materials), that demonstrates efficient separation of xylene isomers with the adsorption preference sequence of *p*X > *m*X > *o*X. Its *p*X/*m*X, *p*X/*o*X, and *m*X/*o*X selectivities are as high as 4.2, 24.4, and 5.8, respectively, attributed to a combined thermodynamic and kinetic effect.

Results and discussion

Calcium-based MOFs (Ca-MOFs) are advantageous for adsorption related applications because of their gravimetric benefit and relatively high stability. However, most of the reported Ca-MOFs feature low-dimensional structures, or high-dimensional dense structures. Three-dimensional (3D) Ca-MOFs with permanent porosity are relatively rare (Table S1†).[12] Here, HIAM-201 was synthesized *via* a solvothermal reaction of $CaCl_2$ and H_4tcpp in ethanol at 120 °C for 2 days, which yielded block-shaped colourless crystals (see the ESI† for synthesis details). Single-crystal X-ray diffraction analysis revealed that the compound crystallizes in a triclinic crystal system with a space group of *P*. Ca^{2+} ions are either 6- or 7-coordinated with an octahedral or pentagonal bipyramid geometry. It is noteworthy that the Ca^{2+} metal centres are coordinated exclusively with carboxylates from H_4tcpp and no coordinated solvents are observed. This is relatively rare for Ca-MOFs as water/solvent molecules tend to occupy one or more coordination sites of Ca^{2+} as a result of its high hydration energy.[12] The structure of HIAM-201 is built on one-dimensional (1D) $[Ca_3(COOH)_2(COO)_6]_n$ chains, which are interconnected by organic linkers to form the final 3D structure with a **deh1** topology (Fig. 1 and S1†).[13] Three out of four carboxylates in each H_4tcpp linker are deprotonated, with one remaining undeprotonated, but all four carboxylates are coordinated to Ca^{2+} centers. The structure possesses 1D open channels along both *a* and *b* axes, with a diameter of ~6.5 Å (H–H, excluding vdw radii). It should be mentioned that the structure of HIAM-201 is totally different from that of Ca(H_2tcpb) built on H_4tcpb (H_4tcpb = 2,3,5,6-tetrakis(4-carboxyphenyl)-benzene), which is similar to H_4tcpp but with a benzene core instead of pyrazine.[14] Unlike H_2tcpb^{2-} which adopts a planar configuration when rigidified in Ca(H_2-tcpb), $Htcpp^{3-}$ is no longer planar in the crystal structure of HIAM-201 (Fig. S2†).

The porosity of HIAM-201 was studied by N_2 adsorption at 77 K. The compound can be activated by direct heating at 150 °C. It shows a type I adsorption profile for N_2 with a saturation capacity of 159 $cm^3\ g^{-1}$, yielding a BET surface area of 604 $m^2\ g^{-1}$ and a pore volume of 0.24 $cm^3\ g^{-1}$ (Fig. S3†). The surface area of HIAM-201 is among the highest for Ca-MOFs, only slightly lower than that of Ca-BTB (Table S1†).[15] DFT pore size distribution analysis reveals that the compound has a uniform pore size of 6–7 Å, consistent with the value measured from its crystal structure (Fig. S4†).

Ca-MOFs, particularly those without coordinated solvents, generally feature robust structures because of the high charge density of calcium metal which leads to strong, ionic-like bonds with organic linkers. We thus examined the stability of the title compound under various conditions. As expected, the material remained intact after being exposed to open air at 250 °C for

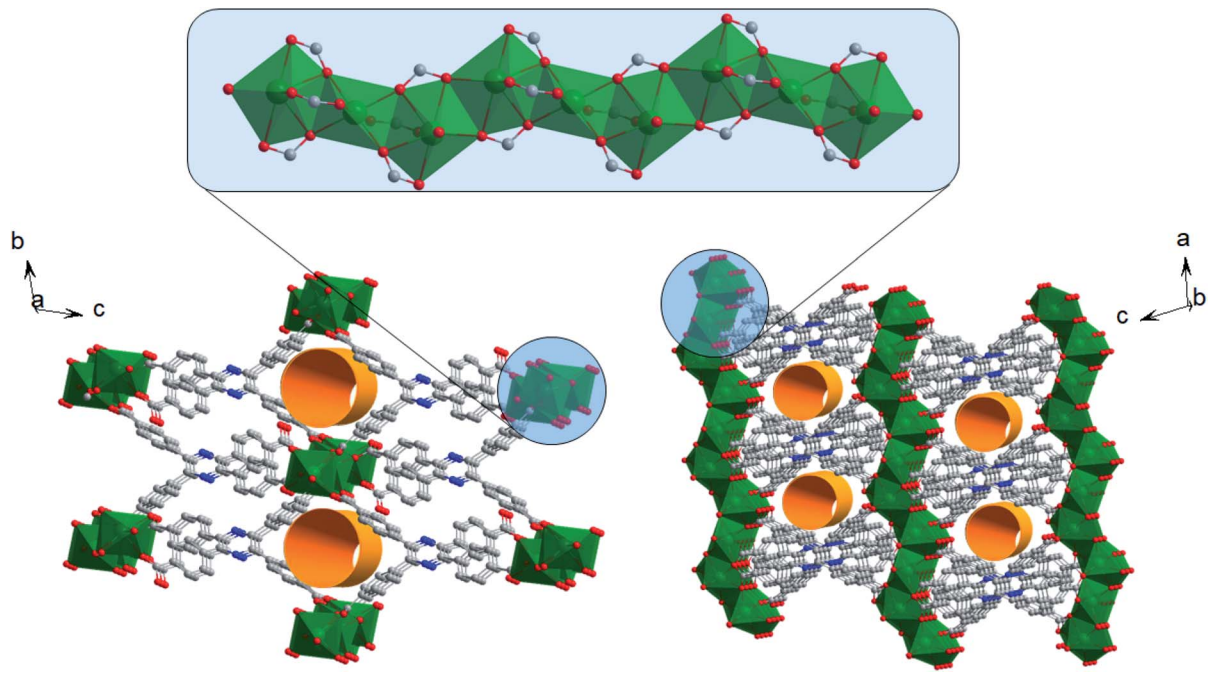

Fig. 1 3D crystal structure of HIAM-201 showing 1D open channels along the *a* axis and *b* axis, and the 1D inorganic chain. Ca: green polyhedra, O: red, N: blue, C: grey, and hydrogen atoms are omitted for clarity.

a week, indicating its high thermal stability and exceptional resistance to moisture (Fig. S5†). Thermogravimetric analysis (TGA) displayed a plateau up to 400 °C before a notable weight loss associated with structural decomposition and the TGA curve of the activated HIAM-201 revealed that no notable weight loss was observed before 400 °C (Fig. S6†). In addition, the synthesis of HIAM-201 can be easily scaled up by 10 times in lab reactions and the product retains the same crystallinity as that of the small-scale reactions (Fig. S8†).

The robust framework, high surface area, and suitable pore dimensions of HIAM-201 encouraged us to explore its capability as an adsorbent for separation of xylene isomers. We selected xylene isomers because their molecular dimensions, particularly those of *o*X and *m*X, are close to the pore size of the MOF. Adsorption isotherms of xylene isomers were collected at 120–150 °C, the temperatures relevant to industrial processes (Fig. 2a–c). Interestingly, HIAM-201 exhibits different adsorption behaviors toward the three xylene isomers. For *p*X, the adsorption isotherms at different temperatures followed the same trend and the adsorbed amount decreased slightly as a function of increasing temperature (Fig. 2a). In contrast, the adsorption profiles for *m*X and *o*X are distinctly different for the same temperature range. Notable decreases in uptake amounts were observed for *m*X and *o*X when the temperature increased from 120 °C to 150 °C. A comparison of the adsorption isotherms of xylenes at 150 °C suggests that HIAM-201 exhibits a noticeable adsorption preference for *p*X over the other two isomers (Fig. 2d). The adsorption capacity for *p*X was 126.7 mg g^{-1} at 150 °C and 1.2 kPa, notably higher than that for *m*X (61.1 mg g^{-1}) and *o*X (33.8 mg g^{-1}) under identical conditions. Henry constants, which are commonly applied to evaluate gas–solid interactions, were calculated based on the adsorption isotherms at different temperatures (Table S2†). In general, Henry constants followed the trend of *p*X > *m*X > *o*X. For example, Henry constants of *p*X, *m*X, and *o*X were calculated to be 299.0, 61.0, and 24.3 mg/g/kPa at 150 °C, respectively, indicating a descending order of interaction with the MOF.

In light of the comparable dimensions of the channels of HIAM-201 and xylene isomers, we also investigated the adsorption kinetics (Fig. S9†) with a home-modified gravimetric adsorption analyser (see the ESI† for experimental details). At 120 °C and 0.8 kPa, the ratio of their diffusion rate coefficients, $D(p\text{X})/D(m\text{X})/D(o\text{X})$, is 1.89/1.24/1.0, following the same trend as that of their Henry constants. These results indicated that the sequence of adsorption preference by HIAM-201 (*p*X > *m*X > *o*X) observed from the adsorption isotherms, is a result of the synergetic effect of thermodynamics and kinetics. To explore the stability of HIAM-201 in repeated adsorption–desorption cycles, 10 consecutive adsorption–desorption cycles were carried out at 150 °C between 0.8 kPa *p*X vapour and nitrogen. No noticeable loss of adsorption capacity was observed during the 10 cycles (Fig. S10†), suggesting robustness of the framework. IR spectra of pristine HIAM-201 and HIAM-201 loaded with different xylene isomers were collected (Fig. S11†), which suggested no notable changes. PXRD patterns (Fig. S12†) of HIAM-201 loaded with different xylene isomers revealed that

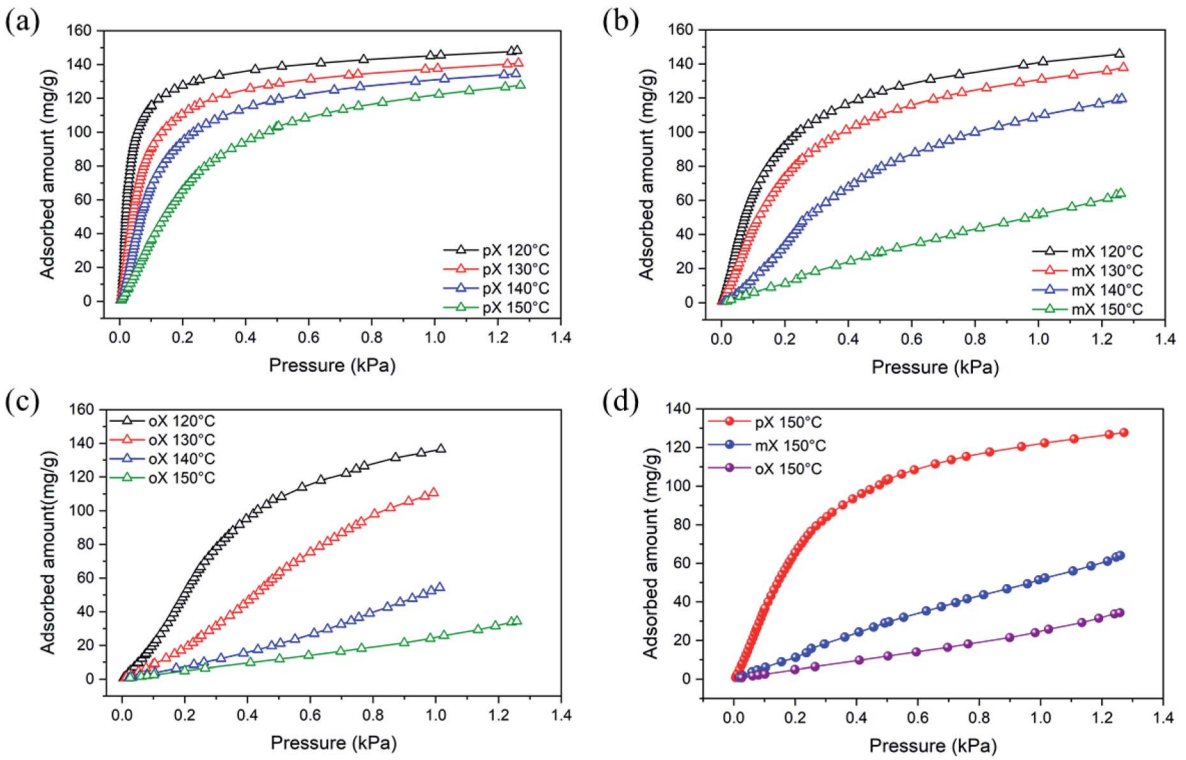

Fig. 2 (a–c) Adsorption isotherms of *p*X (a), *m*X (b), and *o*X (c) at 120–150 °C. (d) Comparison of adsorption isotherms of *p*X, *m*X, and *o*X at 150 °C.

the overall structure was retained upon loading of different guest molecules. A shift of the doublet peak to a lower angle at around $2\theta = 8°$ has been observed for HIAM-201 loaded with xylenes, which is consistent with their corresponding simulated patterns.

The differences in adsorption capacity and adsorption kinetics of xylene isomers by HIAM-201 suggest that the material may be potentially useful for the separation of these physically and chemically similar molecules. We thus evaluated its separation capability through multicomponent column breakthrough measurements at 150 °C. An equimolar ternary vapor mixture of *p*X, *m*X, and *o*X was passed through a column packed with activated HIAM-201 and the eluted vapor was subjected to gas chromatography (GC) analysis. The breakthrough curves are presented in Fig. 3a, which exhibit a clear separation of the three isomers. The first isomer eluted out was *o*X, which broke out at the 13th minute, followed by *m*X at the 55th minute. In contrast, *p*X was retained in the column for the longest time, and was not detected at the outlet until the 130th minute. The elution sequence of the three isomers is consistent with their adsorption preference by HIAM-201. We calculated the dynamic adsorption selectivities based on the ratios of adsorption capacity of each isomer before breakthrough. The *p*X/*m*X, *p*X/*o*X, and *m*X/*o*X selectivities were 2.45, 10.47, and 4.27, respectively. The values, in particular *p*X/*o*X and *m*X/*o*X selectivities, are notably higher than those of most of the reported adsorbents, including the recently reported benchmark material MFM-300 (Fig. S13†).[10,11] The high adsorption selectivities of HIAM-201 should be attributed to its combined thermodynamically and kinetically controlled effects toward the adsorption of xylene isomers. Three consecutive runs of breakthrough experiments revealed that the separation capability of the material was well retained, indicating once again its high stability with respect to adsorption–regeneration cycles.

To further evaluate the capability of HIAM-201 for the separation of xylene mixtures, we examined the composition of xylenes adsorbed in the pores of the MOF after the adsorption equilibrium was reached. The experiments were carried out using the foregoing gravimetric adsorption analyser used to evaluate the adsorption kinetics. Activated HIAM-201 was exposed to an equimolar ternary *p*X/*o*X/*m*X vapor mixture with a partial pressure of 0.8 kPa (carried by nitrogen) at 150 °C until adsorption equilibrium was reached. Desorption was performed by immersing the xylene loaded MOF sample in *n*-hexane under stirring. The subsequently filtered solution was subjected to GC analysis (Fig. 3b and c). The results suggested that the *p*X/*m*X, *p*X/*o*X, and *m*X/*o*X selectivities were 4.17, 24.25, and 5.80, respectively. The selectivities followed the same trend as that observed in breakthrough experiments, but with higher values. This could be attributed to the fact that the adsorbed *o*X and *m*X may be substituted by the more favored *p*X when approaching sufficient equilibrium, leading to higher adsorption selectivities. To evaluate the performance of HIAM-201 in separating *m*X and *o*X, a parallel experiment was carried out with an equimolar binary mixture of *m*X and *o*X as the feed instead of the ternary mixture. Following identical procedures, the *m*X/*o*X selectivity was calculated to be 4.16, indicating the notable preference of *m*X over *o*X and its capability for the separation of the two isomers.

Preferential adsorption of *m*X over *o*X by MOFs was rarely observed in previous studies because of their similar molecular geometries and kinetic diameters. The high *m*X/*o*X adsorption selectivity of HIAM-201 should be attributed to the higher adsorption affinity and adsorption rate of the former. To further understand the adsorption preference of *m*X over *o*X, computational simulations (see the ESI† for details) were performed to evaluate their binding energies with the framework. Two adsorption sites were identified for both *m*X and *o*X in the channels of HIAM-201 (Fig. S14†), and the binding energy calculations performed at both sites indicated that *m*X has stronger binding with the framework as compared to *o*X. The highest binding energies of the two isomers are observed at different sites within the MOF. *m*X binds strongest at site-1 (channels along the *a* axis) with a binding energy of 115.05 kJ mol^{-1} and *o*X has the highest binding energy of 108.87 kJ mol^{-1} at site-2 (channels along the *b* axis). The difference in binding energies further explained why the adsorption of *m*X is more favored over *o*X by HIAM-201.

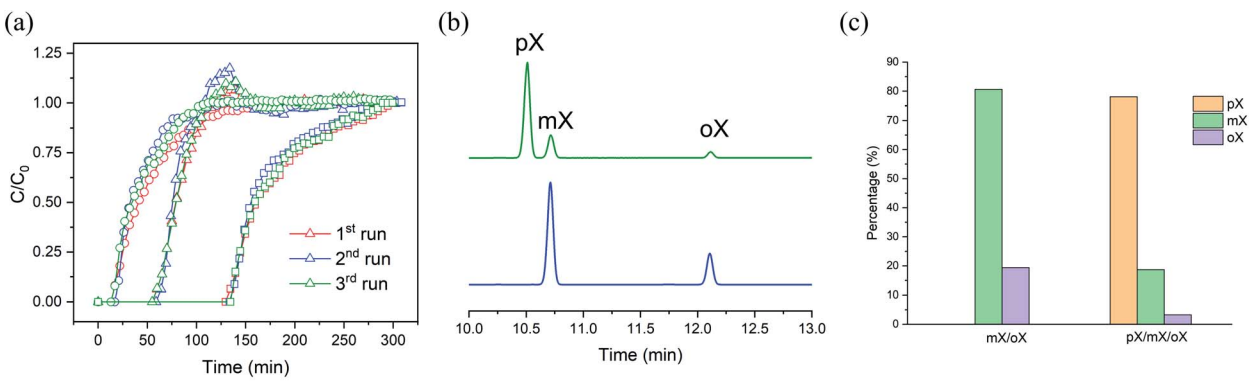

Fig. 3 Separation of xylene mixtures using HIAM-201. (a) Breakthrough curves for the three consecutive runs of multicomponent column breakthrough experiments for xylene isomers at 150 °C, squares: *p*X, triangles: *m*X, and cirles: *o*X. (b) GC analysis of desorbed xylenes from HIAM-201 saturated with equimolar xylene vapors (blue: *m*X/*o*X; green: *p*X/*m*X/*o*X) at 150 °C. (c) Integration of GC peaks.

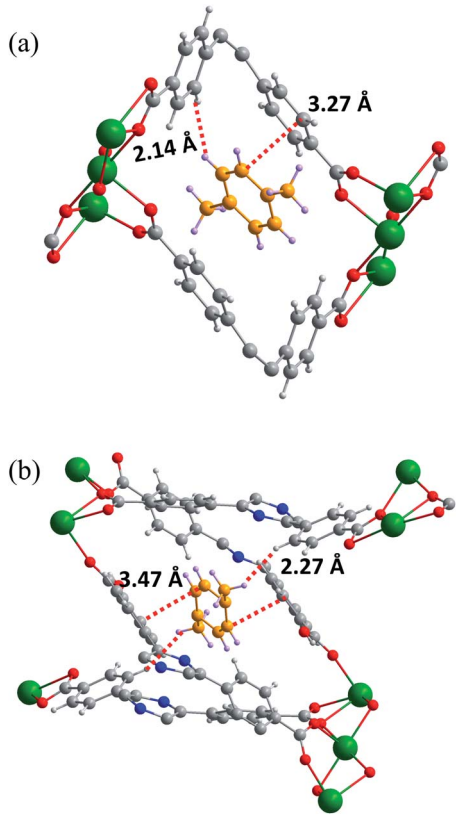

Fig. 4 Adsorption sites of *p*X in the channel along the *a* axis (a) and the channel along the *b* axis (b) of HIAM-201, determined by single-crystal X-ray diffraction.

To explore the guest–MOF interactions at the molecular level, we attempted to obtain the crystal structures of HIAM-201 loaded with xylenes. Thorough guest exchange of ethanol, the initial solvent residing in the pores of HIAM-201, with *p*X (or *m*X, *o*X) afforded *p*X (or *m*X, *o*X) loaded HIAM-201, denoted as *p*X@HIAM-201 (or *m*X@HIAM-201, *o*X@HIAM-201). The crystal structures of xylene loaded HIAM-201 were determined through single-crystal X-ray diffraction (Fig. S15–S17†). Taking *p*X@HIAM-201 as an example, *p*X molecules were adsorbed in both channels along *a* and *b* axes (Fig. 4), interacting with the framework *via* van der Waals forces. The closest H···H and C···C distances between *p*X and the framework are 2.14 and 3.27 Å, respectively, indicating notable guest–host interactions. The other two isomers, *m*X and *o*X, reside at positions similar to that of *p*X, packed with certain disorders (Fig. S16 and S17†). The guest–host vdW interaction is similar for different xylene isomers. The difference in adsorption affinity could be attributed to the degree of matching between the shape of xylene molecules and the channel shape of HIAM-201.

Conclusions

Adsorptive separation of xylene isomers, in particular *m*X and *o*X with a similar molecular geometry and dimension, is challenging but industrially important. It has stringent requirements with respect to the pore structure of the adsorbents. In this work, we present a new calcium-based microporous MOF, HIAM-201, with an optimal pore size and shape for the separation of xylene isomers. Its adsorption preference follows the sequence of *p*X > *m*X > *o*X, with high adsorption selectivities as evidenced by multicomponent adsorption studies. Our studies reveal that the high adsorption selectivities are the results of synergetic effects of thermodynamics and kinetics.

Author contributions

H. W., Y. H., and J. L. conceived the idea. Y. L., L. Y., K. Z., and W. Y. performed the synthesis, characterization, single-component adsorption study, and structure determination. J. Z., X. D., Q. G., and X. H. performed the column breakthrough and GC analysis. H. P. and T. T. carried out the computational calculations. H. W. wrote the paper and all authors contributed to the discussion and final proof of the manuscript.

Conflicts of interest

There are no conflicts to declare.

Acknowledgements

We thank the National Natural Science Foundation of China (21901166), Guangdong Natural Science Foundation (2019A1515010692), and Shenzhen Science and Technology Progrm (No. JCYJ20190809145615620, and RCYX20200714114539243). Work in the US was entirely supported by the U.S. Department of Energy, Office of Science, Office of Basic Energy Sciences under Award No. DE-SC0019902.

Notes and references

1 R. Lively, *Nature*, 2016, **532**, 435–437.
2 J.-R. Li, R. J. Kuppler and H.-C. Zhou, *Chem. Soc. Rev.*, 2009, **38**, 1477–1504.
3 (*a*) H. Furukawa, K. E. Cordova, M. O'Keeffe and O. M. Yaghi, *Science*, 2013, **341**, 1230444; (*b*) H. Wang, Y. Liu and J. Li, *Adv. Mater.*, 2020, **32**, 2002603; (*c*) Z. Bao, G. Chang, H. Xing, R. Krishna, Q. Ren and B. Chen, *Energy Environ. Sci.*, 2016, **9**, 3612–3641; (*d*) K. Adil, Y. Belmabkhout, R. S. Pillai, A. Cadiau, P. M. Bhatt, A. H. Assen, G. Maurin and M. Eddaoudi, *Chem. Soc. Rev.*, 2017, **46**, 3402–3430.
4 X. Yang, H.-L. Zhou, C.-T. He, Z.-W. Mo, J.-W. Ye, X.-M. Chen and J.-P. Zhang, *Research*, 2019, **2019**, 9463719.
5 Z. Jin, H.-Y. Zhao, X.-J. Zhao, Q.-R. Fang, J. R. Long and G.-S. Zhu, *Chem. Commun.*, 2010, **46**, 8612–8614.
6 S.-Q. Wang, S. Mukherjee, E. Patyk-Kaźmierczak, S. Darwish, A. Bajpai, Q.-Y. Yang and M. J. Zaworotko, *Angew. Chem., Int. Ed.*, 2019, **58**, 6630–6634.
7 M. I. Gonzalez, M. T. Kapelewski, E. D. Bloch, P. J. Milner, D. A. Reed, M. R. Hudson, J. A. Mason, G. Barin, C. M. Brown and J. R. Long, *J. Am. Chem. Soc.*, 2018, **140**, 3412–3422.
8 (*a*) Z. He, Y. Yang, P. Bai and X. Guo, *J. Ind. Eng. Chem.*, 2019, **77**, 262–272; (*b*) R. E. Osta, A. Carlin-Sinclair, N. Guillou,

R. Walton, F. Vermoortele, M. Maes, D. Vos and F. Millange, *Chem. Mater.*, 2012, **24**, 2781–2791.
9 L. Chen, D.-D. Zhu, G.-J. Ji, S. Yuan, J.-F. Qian, M.-Y. He, Q. Chen and Z.-H. Zhang, *J. Chem. Technol. Biotechnol.*, 2018, **93**, 2898–2905.
10 X. Cui, Z. Niu, C. Shan, L. Yang, J. Hu, Q. Wang, P. C. Lan, Y. Li, L. Wojtas, S. Ma and H. Xing, *Nat. Commun.*, 2020, **11**, 5456.
11 X. Li, J. Wang, N. Bai, X. Zhang, X. Han, I. da Silva, C. G. Morris, S. Xu, D. M. Wilary, Y. Sun, Y. Cheng, C. A. Murray, C. C. Tang, M. D. Frogley, G. Cinque, T. Lowe, H. Zhang, A. J. Ramirez-Cuesta, K. M. Thomas, L. W. Bolton, S. Yang and M. Schröder, *Nat. Commun.*, 2020, **11**, 4280.
12 S. Xian, Y. Lin, H. Wang and J. Li, *Small*, 2021, **17**, 2005165.
13 J.-P. Mo, F. Bigdeli, Y. Ying, C.-Q. Zhu, M. Zhu, Y.-S. Li, X.-H. Li, H.-P. Xiao, A. Morsali and A. Ramazani, *Polyhedron*, 2019, **158**, 144–153.
14 (*a*) H. Wang, X. Dong, E. Velasco, D. H. Olson, Y. Han and J. Li, *Energy Environ. Sci.*, 2018, **11**, 1226–1231; (*b*) X. Chen, A. M. Plonka, D. Banerjee, R. Krishna, H. T. Schaef, S. Ghose, P. K. Thallapally and J. B. Parise, *J. Am. Chem. Soc.*, 2015, **137**, 7007–7010.
15 K. Noh, N. Ko, H. J. Park, S. Park and J. Kim, *CrystEngComm*, 2014, **16**, 8664–8668.